All changes are highlighted in version 2.

Automated analysis of microplastics based on vibrational spectroscopy: Are we measuring the same metrics?

Mingtan Dong[1*], Zhenbing She[2,4], Xiong Xiong[3], Zejiao Luo[1**]

1 School of Environmental Studies, China University of Geosciences, Wuhan 430078, China

2 State Key Laboratory of Biogeology and Environmental Geology, China University of Geosciences, Wuhan 430078, China

3 State Key Laboratory of Freshwater Ecology and Biotechnology, Institute of Hydrobiology, Chinese Academy of Sciences, Wuhan 430072, China

4 School of Earth Sciences, China University of Geosciences, Wuhan 430074, China

ABSTRACT: The traditional manual analysis of microplastics has been criticized because it is labor intensive, inaccurate for identifying very small microplastics, and difficult to standardize or compare. There are already three automated analysis strategies for microplastics based on vibrational spectroscopy, laser direct infrared (LDIR)-based particle analysis, Raman-based particle analysis, and focal plane array-Fourier transform infrared (FPA-FTIR) imaging. We compared the performances of these strategies in terms of their quantification, detection limit, size measurement, and material identification accuracy and analysis speed by analyzing the same standard and environmental samples. Unfortunately, the automated analysis strategies are not consistent in terms of the quantification and material identification results. The number of particles smaller than 60 μm recognized by Raman-based particle analysis is far greater than that recognized by LDIR-based particle analysis. Raman-based particle analysis has a submicrometer detection limit but should not be used in the automated analysis of microplastics in environmental samples because of the strong fluorescence interference. LDIR-based particle analysis provides the fastest analysis speed, but we suggest using a reliable detection limit of approximately 60 μm and considering the material identification results and reference database used because the wavenumbers LDIR spectra are in the range of 975-1800 cm^{-1}. FPA-FTIR imaging provides relatively reliable quantification and material identification for microplastics in environmental samples but might provide an imprecise description of the particle shapes. Optical photothermal infrared (O-PTIR) spectroscopy can detect submicron-sized microplastics (0.5-5 μm) but has not been automated. As a technological advancement, automated analysis of microplastics should be encouraged, but we need to foster the strengths and circumvent the weaknesses of different strategies. The automated analysis of microplastics should be further validated and standardized.

It is almost certain that microplastics, plastics smaller than 5 mm[1], exist in every environment of Earth's surface[2], and all species may be exposed to microplastics[1,3]. Microplastics are emerging pollutants known for their interaction with other pollutants[4] and potential toxicity to organisms[5]. Therefore, the accurate and efficient analysis of microplastics in different matrices is important and the first step in the work to assess and describe microplastic pollution. The entire analysis process of microplastics includes sampling, pretreatment, identification and quantification, but the 'analysis' in this study is specially defined as the only identification and quantification of microplastics.

The traditional manual analysis of microplastics requires an operator to visually recognize, count, and measure microplastics under a stereomicroscope. Then, these suspected microplastics will be transferred into Fourier transform infrared (FTIR) spectroscopy, Raman spectroscopy, or pyrolysis-gas chromatography−mass spectrometry (Pyr-GC-MS) instruments to identify each their polymer type[6]. Particles smaller than 100 μm are challenging to recognize visually[7] and transfer into an instrument to identify their material types. Nile red staining can assist visual recognition of microplastics but cannot identify polymer types[8]. In addition, most studies consider only a part of the visually recognized microplastics to identify their polymer types[9,10], but only 1.4% of suspected microplastics identified visually were confirmed as polymers[11]. The traditional manual analysis methods of microplastics are labor intensive, inaccurate, easily affected by operator-related factors, and it remains difficult to detect microplastics smaller than 100 μm. However, small microplastics usually have a higher abundance in the environment[2] and stronger toxicological effects[12].

We define the term 'automated analysis of microplastics' as a strategy that could automatically recognize, count, measure the size of, and identify the material types of microplastics to quantify them. Such an approach should have low detection limits and be labor-free, efficient, and accurate. Although technologies such as secondary ion mass spectrometry (SIMS)[13] and single particle-inductively coupled plasma mass spectrometry (SP-ICP-MS)[14] have been applied to detect microplastics in recent years, they are difficult to apply in environmental samples[14]. In contrast, the automated analysis of microplastics based on vibrational spectroscopy (Raman and infrared) is more compatible with existing studies and sample pretreatment methods. There are three strategies for the automated analysis of microplastics: laser direct infrared (LDIR)-based particle analysis[15], Raman-based particle analysis[16], and focal plane array (FPA)-FTIR imaging[2,17-19]. They are based on different instruments and principles. The problem with the traditional manual analysis of microplastics has been that it is challenging to compare the quantitative results of different studies[20-22]. Naturally, a new question arises: Are we measuring the same metrics when

using these different strategies to analyze microplastics automatically?

Therefore, for technique validation, we designed a comparative study of the performance of these strategies in the automated analysis of microplastics. The same standard microplastic sample and environmental microplastic sample were analyzed with different strategies. The comparative targets include the detection limit, size measurement, material identification, quantification results, and analysis speed. Additionally, the performance of optical photothermal infrared (O-PTIR) spectroscopy[23,24] and Raman mapping (Raman imaging)[25,26] was compared with that of Raman-based particle analysis for detecting microplastics smaller than 5 μm. The sample preparation requirements of different strategies were also discussed.

EXPERIMENTAL SECTION

Microplastic sample preparation

Eight virgin microplastic particle powders (Table S1) were purchased from Ante Plastic Materials Co., Ltd. (China). Different from the commonly used polystyrene microspheres[27], these standard microplastic powders are irregular particles, including polyethylene (PE), polyethylene terephthalate (PET), polyvinyl chloride (PVC), polyamide (PA), and polystyrene (PS), with particle sizes ranging from approximately 1 μm to 300 μm. Then, these different microplastic powders with different polymer types and sizes were mixed in absolute ethyl alcohol to be used as the standard microplastic sample (Fig. 1).

Environmental microplastics (Fig. S1) were extracted with $ZnCl_2$ (1.7 g·cm^{-3}) from the soil of one of the world's largest plastic waste recycling bases[28]. Then, the environmental microplastics were filtered through 150 mesh and 500 mesh metal sieve stacks. Finally, environmental microplastics with a size of approximately 30-100 μm were rinsed from the sieve with absolute ethyl alcohol and used as the environmental sample (Fig. 1).

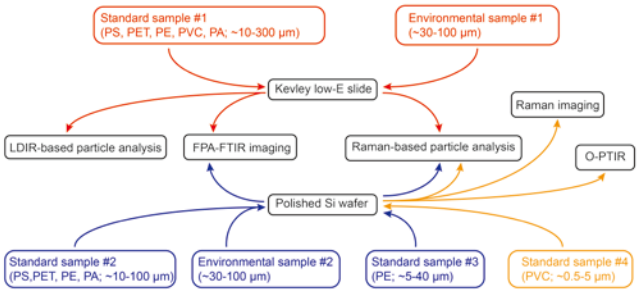

Figure 1. Flow chart of the comparative study between different strategies for the automated analysis of microplastics.

LDIR-based particle analysis

Agilent 8700 LDIR (Agilent Solutions, Inc., USA) is a novel technique and is different from traditional FTIR. It uses a mid-IR quantum cascade laser (QCL) as the light source. Infrared light from the QCL is directed to the sample, then reflected by the sample, and directed to a thermoelectrically cooled mercury-cadmium-telluride (MCT) detector. Agilent 8700 LDIR only accepts glass slides for loading samples. The particles dispersed in the ethanol solution are dropped onto Kevley low-E slides (Fig. S2a). First, the instrument obtains a bright image with a large-field-of-view camera (resolution of approximately 24 μm). Then, it uses single wave light (1800 cm^{-1}) with a spatial resolution of 5.5 μm (1 cm/1800 cm^{-1}) to survey, count, locate and measure the particles in this image. Third, it measures the infrared spectrum of each particle in reflection mode. Finally, Clarity software (version 1.3.42, Agilent) is used to automatically compare the spectrum with the reference spectral library to identify the material types. Spectra with a match quality smaller than 0.65 were listed as 'Undefined'. The reference spectral library contains polymer and nonpolymer materials (e.g., coal, alkyd varnish, and chitin). After, if essential, clearer images of the particles of interest can be acquired under the objective (resolution 1 μm). In this work, the detection threshold was set to 20 μm. The spectral range was 975-1800 cm^{-1} with a resolution of 0.5 cm^{-1}. The image of the particles in environmental sample #1 were reacquired under the objective after regular analysis.

Raman-based particle analysis

WITec ParticleScout (version 5.3.14.106) is software used with a WITec alpha300 R confocal Raman imaging system (WITec GmbH, Germany). First, it obtains a large-area image by the image-stitching and focus-stacking function. Then, it surveys, measures, and locates particles in this image. Next, it acquires the Raman spectrum of each particle with the Autofocus setting and identifies them by linking the WITec TrueMatch database. The logic of WITec ParticleScout in detecting microplastics is similar to that of Agilent 8700 LDIR.

The WITec alpha300 R spectroscope used was equipped with a 532 nm laser. The grating used had a groove density of 600 lines per millimeter and a Blaze wavelength (BLZ) of 500 nm. The Raman shift ranged from 0-4000 cm^{-1}. A 20-magnification darkfield objective (EC Epiplan-Neofluar HD, Zeiss) with 0.5 numerical aperture (NA) was used in the analysis of standard samples #1, #2, and #3 and environmental samples #1 and #2 (Fig. 1). A 100-magnification brightfield objective (EC Epiplan-Neofluar Dic, Zeiss) with 0.9 NA was used to analyze standard sample #4 (Fig. 1). The pixel sizes of visible light images taken under the 20× and 100× objectives were 0.61 μm and 0.12 μm, respectively. According to the Rayleigh criterion, the lateral resolution (0.61λ/NA) of the Raman spectra acquired under the 20× and 100× objectives were 0.65 μm and 0.36 μm, respectively, and the axial resolutions in the air (1.4λ/NA^2) were 3 μm and 0.92 μm, respectively. The vignetting of the image was corrected in real time to prevent it from affecting particle recognition. The threshold of finding particles from the dark field images was automatically set by ParticleScout. The spectrum of each particle was automatically acquired with signal optimization settings (integration time: 1 s; accumulation number: 3 or 5 times; and laser power: 5 mW). Autofocus setting was performed for the Raman shift range of 2800-3200 cm^{-1}, and the steps under the 20× and 100× objectives were set to 2 μm and 0.2 μm, respectively. The Raman Database of Weathered Microplastics built in our previous study[28] and a commercial polymer database (ST Japan 5.2) containing 4568 Raman spectra were used to confirm polymer types through WITec TrueMatch Database software. Spectra with a hit index quality (HQI) smaller than 60 were listed as 'Unknown'. In addition, the Raman mapping performed to detect the microplastics in standard sample #4 followed the same Raman spectroscopy approach. ParticleScout was also used to count and measure particles from the Raman map.

Additionally, Raman spectra are easily affected by fluorescence interference[28,29]. Another two WITec alpha300 R instruments equipped with 488 and 785 nm lasers were used to measure the Raman spectra of some particles in the environmental samples to compare the performance of different lasers in reducing fluorescence interference.

FPA-FTIR imaging

A LUMOS II FT-IR imaging microscope (Bruker Optics GmbH, Germany) equips 32×32 focal-plane array detectors and can acquire 1024 infrared spectra in a single scan at a minimum spatial resolution of 5 μm. The logic of FPA-FTIR imaging in detecting microplastics is different from the particle recognition-spectrum measurement mode of particle analysis. FPA-FTIR spectroscopy detects microplastics from hyperspectral chemical imaging rather than visible light imaging or single-wave imaging. As early as 2015, FPA-FTIR imaging was used to identify microplastics from environmental matrix[11,18,30]. However, the visualization of microplastics based on the integration of a single peak cannot cope with different polymer types, and the considerable amount of data makes this approach unable to be widely used in the automated analysis of microplastics[31]. Within the past two years, multivariate statistics, data mining, and machine learning methods, such as principal component analysis[32], cluster analysis[32], random decision forest (RDF) classifiers[33], and partial least squares discriminant analysis[17], were applied to process hyperspectral imaging. These methods make it possible to reduce the dimensionality of hyperspectral infrared imaging and detect and quantify microplastics. Two software programs, siMPle developed by Primpke et al.[34] and Purency Microplastics Finder (Purency GmbH, Austria), can be applied in processing FPA-FTIR imaging.

In this work, the FPA detectors measured the infrared spectra in reflection mode with a spectral resolution of 8 cm^{-1} and 2 scans. The wavenumber ranged from 750-4000 cm^{-1}. Except for standard sample #3 (Fig. 1), which was measured at a spatial resolution of 5 μm (no binning), the other samples (Fig. 1) were measured at a spatial resolution of 10 μm (2×2 binning). The background was measured with the same parameters and was subtracted from the results. Then, the hyperspectral data were imported into Purency Microplastics Finder (version 3.49) running with a machine learning model (version PMF_R2021a) based on the RDF classifiers[33] to detect, measure and classify the microplastics. The spectra from 1250-3600 cm^{-1} were used for the Purency calculations. This process only detected the microplastics, and other particles were listed as 'Unknown'.

The machine learning model in Purency Microplastics Finder was trained with the transmission spectrum imaging data obtained with an aluminum oxide filter[33]. Although the Kevley low-E slides were designed for reflective infrared measurements and were used in the LDIR spectral measurements, the infrared spectra of the Kevely low-E slides (Fig. S3b) differed from the infrared spectra of aluminum oxide (Fig. S3a) and were not compatible for the Purency Microplastics Finder. Therefore, the edges of the microplastics loaded on the Kevley low-E slide are poorly recognized (Fig. S5). The quantification and size measurement of standard sample #1 and environmental sample #1 acquired by the Bruker-Purency Microplastics Finder strategy were not compared with those acquired by the LDIR-based or Raman-based particle analysis; only the results of the material identification and operational speed were compared. Another three samples were loaded on a polished silicon wafer (Fig. S2b) to compare the quantification and size measurement results between the FPA-FTIR imaging and Raman-based particle analysis strategies (Fig. 1). The FPA measurement of the silicon wafer still used the reflection mode based on the consideration of measurement consistency. We noticed that the FTIR reflection spectrum of the polished silicon wafer had a more negligible absorbance than the transmission spectrum (Fig. S4).

Note that the FPA-FTIR imaging strategy was not run under the optimal settings to meet the sample preparation requirements of different strategies, which may adversely affect the results.

O-PTIR measurements

O-PTIR spectra and imaging was measured on a commercial instrument, mIRage (Photothermal Spectroscopy Corp., USA). mIRage system used in this study equipped a QCL (MIRcat-QT, DRS Daylight Solutions Inc, USA) with the wavenumber ranged from 800-1800 cm^{-1}, but the principles and working mode of O-PTIR are different from QCL-IR (LDIR). The photothermal expansion in the sample surface caused by the absorption of infrared radiation will change the intensity of the reflected or scattered light, and the intensity change of the visible light is proportional to the absorption of infrared radiation[35,36]. O-PTIR uses a visible light probe to detect the photothermal event induced by the incident infrared radiation[35,36]. mIRage equipped a 532 nm laser as the probe and a 40× objective (0.78 NA), so the resolution of O-PTIR can be approximately 500 nm. Besides, mIRage equipped an iHR320 imaging spectrometer (Horiba, Japan) and could acquire Raman spectrum excited by the 532 nm laser at the same time, same spot, and same resolution in the measurement of O-PTIR spectrum.

We used mIRage to measure the O-PTIR and Raman spectra of standard PVC particles ranged from about 0.5-5 μm (Figure 1) and used the single wavenumber infrared light to map the microplastics. The IR power, probe power, duty cycle, scan rate, and step size were adjusted and optimized based on the demand. Hyperspectral imaging was not performed because it was time-consuming.

Quality assurance and quality control

The LDIR-based particle analysis strategy analyzed the samples first. Then, the samples were stored in separate hermetic boxes and were manually transported to different laboratories instead of being transported by express mail. We tried our best to avoid vibration and collision during transport. All the instrument analyses were completed within one week in May 2021 to ensure the consistency of the particles. The area of Raman-based particle analysis and FPA-FTIR imaging was slightly larger than those of the LDIR-based particle analysis, which made it easier to compare particles. Particles were cross-checked in terms of their position and shape to compare the size measurement and material identification results for the same particle. Two particle size standards of 10.12±0.06 μm (4K-10, Duke Standards, Thermo Scientific, USA) and 100±1.5 μm (4K-100, Duke Standards, Thermo Scientific, USA) were used to validate the size measurement results of the Raman-based particle analysis.

RESULTS AND DISCUSSION

Quantification and detection limits

Since manta and neuston nets are often used in the sampling of microplastics and metal sieves are used for prefiltration[6,22], the width of the particles is used as the size. The number of particles smaller than 60 μm recognized by the LDIR-based particle analysis is much smaller than that recognized by the Raman-based particle analysis (Fig. 2a, c), which means that the LDIR-based particle analysis is not accurate in the quantification of microplastics smaller than 60 μm. Thus, the percentage of microplastics smaller than 60 μm is expected to be underestimated in studies using LDIR-based particle analysis[15,37,38]. The Raman-based particle analysis is based on darkfield images with a resolution of 0.61 μm, which is helpful for recognizing very small particles. For standard sample #1, the quantitative results

of microplastics under Raman-based particle analysis are much higher than those under LDIR-based particle analysis (Fig. 2b). For environmental sample #1, the number of microplastics detected by Raman-based particle analysis is smaller than that detected by LDIR-based particle analysis because the differences in material identification also affect the quantification of the microplastics.

In standard sample #2, the microplastics smaller than 30 μm quantified by Raman-based particle analysis are much more abundant than those quantified by FPA-FTIR imaging (Fig. 2e) because FPA FTIR imaging of standard sample #2 was run with a 10 μm resolution (2×2 binning). In standard sample #3, the microplastics quantified by FPA-FTIR imaging with a 5 μm resolution (no binning) are more similar to those quantified by Raman-based particle analysis (Fig. 2f). However, the number of microplastics in environmental sample #2 detected by Raman-based particle analysis is much lower than that detected by FPA-FTIR imaging (Fig. 2g), similar to the difference observed for environmental sample #1 between the LDIR-based particle analysis and Raman-based particle analysis results (Fig. 2d).

The difference in the quantitative results is affected by the detection limit, particle recognition, size measurement, and material identification of the microplastics. Different strategies have different detection limits (Fig. 2h). We do not suggest using the lowest detection limit to quantify microplastics because these strategies are often inaccurate for quantifying microplastics close to the detection limit (Fig. 2a, c). We recommend using a more reliable detection limit based on the consideration of the spatial resolution of the spectra and the size measurement (Fig. 2h).

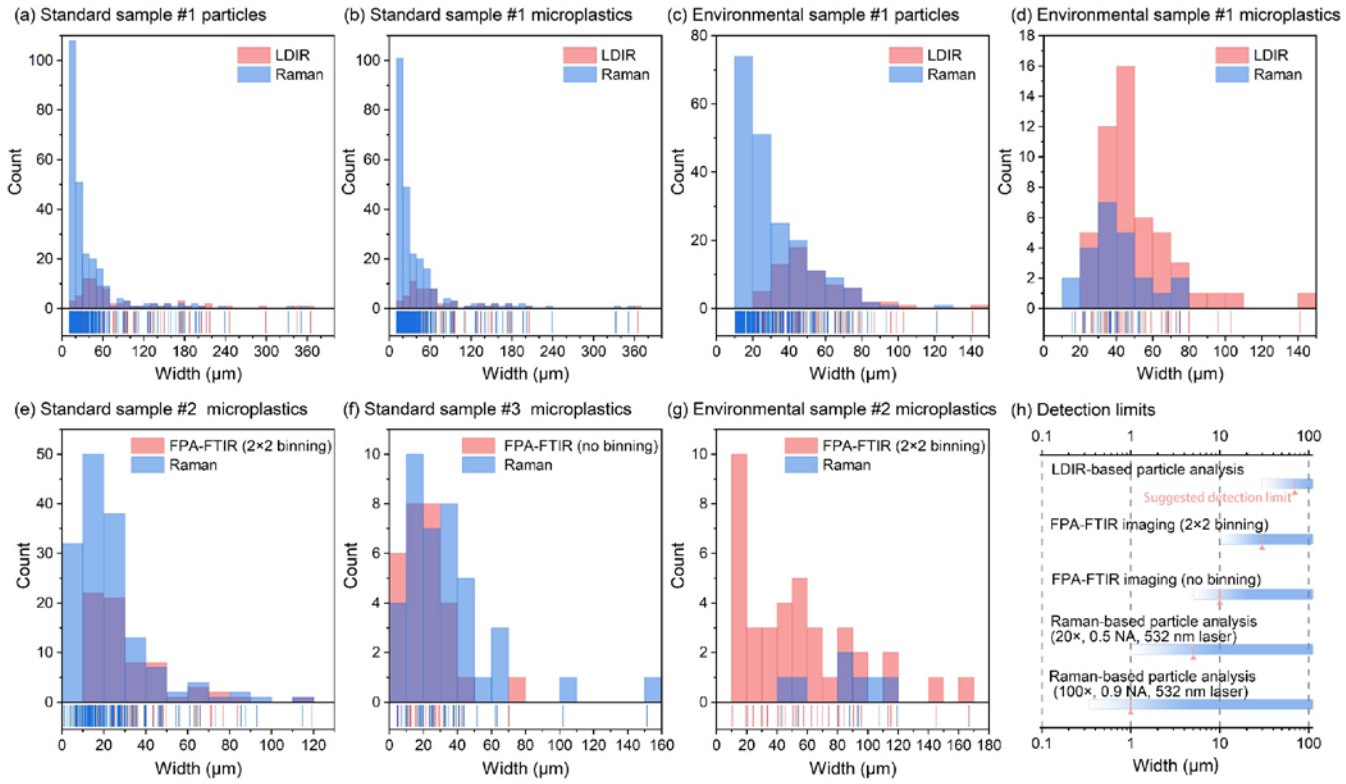

Figure 2. Quantification results of different strategies for the same sample (a-g) and the detection limits of different strategies (h).

Size measurement

The measurement result of the Raman-based particle analysis for the spherical PS standard with a particle size of 10.12±0.06 μm is 12.23±0.74 μm, and the measurement result for the standard with a particle size of 100±1.5 μm is 97.68±4.46 μm. It is difficult to find the equatorial plane of spherical particles. The particle brightness may influence edge recognition in creating a particle mask. Generally, the size measurement of the Raman-based particle analysis is accurate. The size measurement of the LDIR-based particle analysis is linearly correlated to the Raman-based particle analysis (Fig. S6a, b). However, the slope of the linear fit is not 1, and the intercept is not 0, indicating a difference between the size measurements of Raman-based and LDIR-based particle analysis.

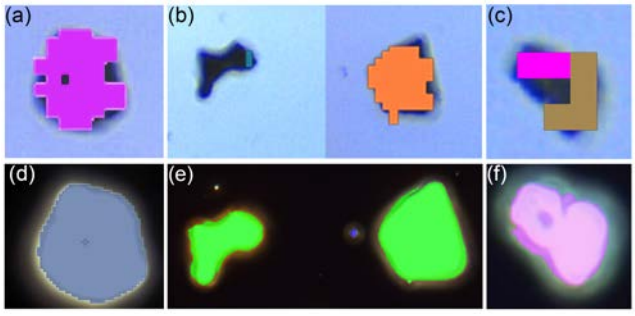

Figure 3. Microplastic masks created by FPA-FTIR imaging (a, b, c) and Raman-based particle analysis (d, e, f). (a, c, d and f) are from the material maps of standard sample #2 (Figs. S8 and S9), but (b) and (e) are from environmental sample #2. The different colors in (a, b, and c) represent different polymer types.

A gap exists between the particle sizes measured by Raman-based particle analysis and FPA-FTIR imaging (Fig. S6c, d, e). The particle sizes measured by FPA-FTIR imaging seem to be

an order or magnitude greater than the resolution. For example, the particle sizes measured under 2×2 binning are often 10 μm to 20 μm (Fig. S6c). Clearly, the particle size measured with a resolution of 10 μm is far less accurate than that measured by Raman-based particle analysis (Fig. 3a, d). Thus, a higher resolution corresponds to a higher accuracy in the size measurement. In addition, the particle size measurement under FPA-FTIR imaging is also related to the recognition of particle edges. The uneven thickness and varying weathering degrees of different spots of one microplastic particle will affect the corresponding infrared spectra; thus, creating particle masks with Purency Microplastics Finder is challenging (Fig. 3b). Although Purency Microplastics Finder allows the users to re-edit the particle mask to improve the accuracy of the particle measurement, this step will increase the workload and was not applied in this study. Raman-based particle analysis is not affected by the inconsistent spectra of the particles themselves (Fig. 3e), but an advantage of FPA-FTIR imaging is that it could distinguish adjacent particles with different polymer types (Fig. 3c), which also could be recognized in one microplastic particle by particle analysis (Fig. 3f).

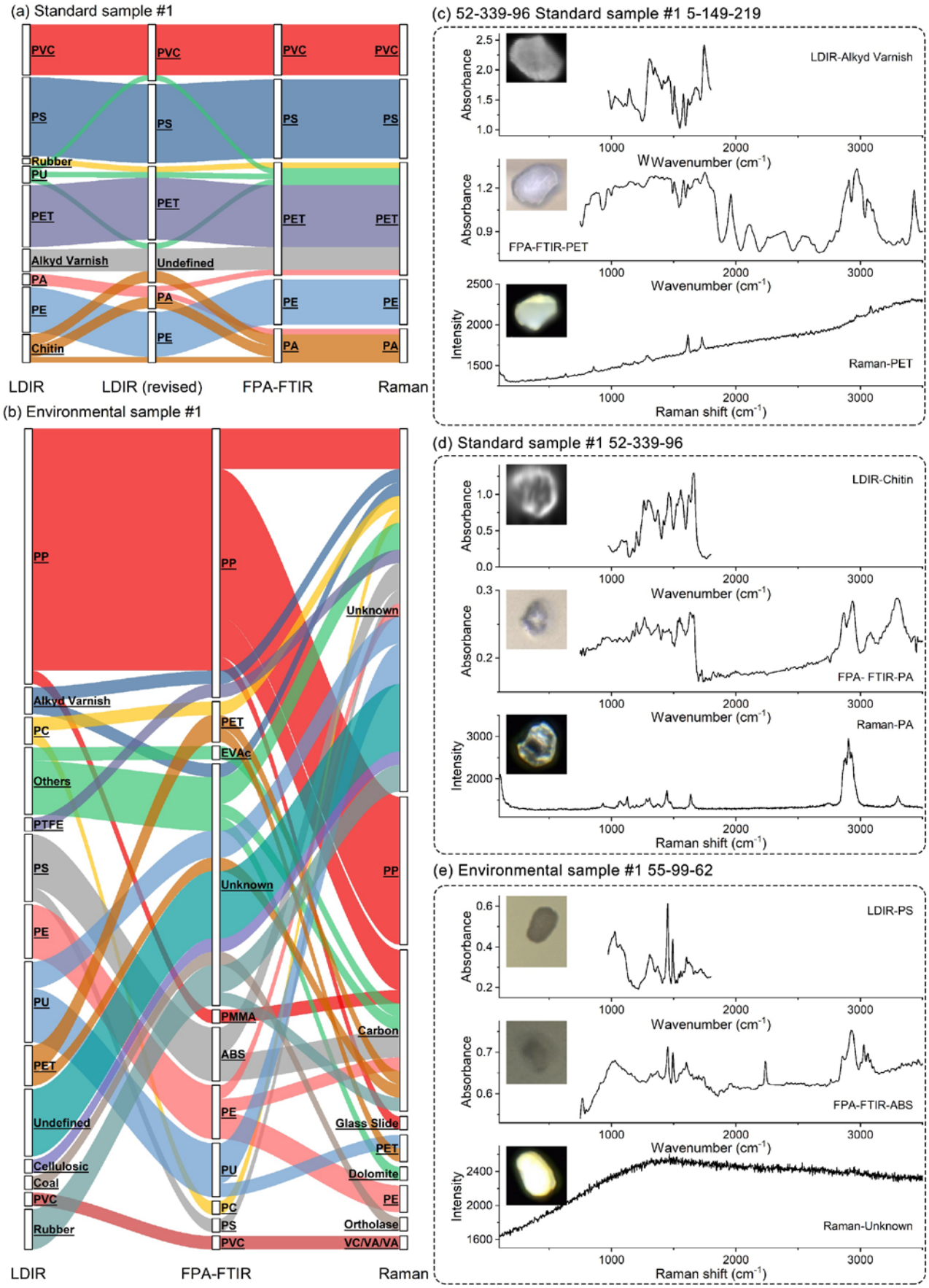

Figure 4. Comparison of the material identification results of standard sample #1 (a) and environmental sample #1 (b) under different strategies. LDIR, FTIR and Raman spectra for the same particle (c, d, e).

Material identification

Raman-based particle analysis and FPA-FTIR imaging are consistent in identifying particles in standard sample #1, but they are inconsistent with LDIR-based particle analysis (Fig. 4a). In the LDIR-based particle analysis, PET may be erroneously classified as alkyd varnish, polyurethane (PU), PA, and rubber, and PA is erroneously classified as chitin (Fig. 4a). In fact, the LDIR spectra of these particles are the same as the FTIR spectra (Fig. 4c, d). The incorrect classification of particles is related to the built-in database of Clarity. Clarity's built-in database includes nonplastic materials such as chitin and alkyd varnish, resulting in overmatching phenomena in standard sample #1. When the nonplastic materials were removed from the library, the revised material identification results of the LDIR-based particle analysis strategy were closer to those of Raman-based particle analysis and FPA-FTIR imaging. In addition, the wavenumber range of the LDIR-based particle analysis is only 975-1800 cm^{-1}, restricting the polymer identification from referring to the stretching vibration of C-H bonds at 2800-3000 cm^{-1}. The FPA-FTIR imaging strategy has a wider wavenumber range, 1250-3600 cm^{-1}, and Raman-based particle analysis has a Raman shift range of 0-4000 cm^{-1}, making material identification more stable.

The difference in material identification of particles in environmental samples between these three strategies is even greater (Fig. 4b). The LDIR- and FTIR-based identification of polypropylene (PP), PE and PU are basically consistent, but the LDIR classifies acrylonitrile butadiene styrene (ABS) as PS because of the stretching vibration of C≡N in ABS located at 2236 cm^{-1}, beyond 975-1800 cm^{-1} (Fig. 4e). There will be a series of changes in the infrared spectrum of weathered microplastics, such as a C-O stretching vibration peak at 1010 cm^{-1}, a C=C stretching vibration peak at 1640 cm^{-1}, and a series of carbonyl stretching vibration peaks at 1680-1800 cm^{-1} [28]. In contrast, the peaks of the C-H stretching vibration of 2800-3000 cm^{-1} of polymers are more robust against weathering[28].

The Raman spectra of weathered microplastics[7,28] and microplastics with pigment additives[29] often have strong fluorescence and cannot be identified (Fig. 4e). Switching lasers usually reduces fluorescence interference, but a single laser cannot cope with the diversity of particles in environmental samples in particle analysis mode. For some particles, 488, 532, and 785 nm lasers cannot obtain effective Raman spectra (Fig. S7d-g), which means that Raman-based particle analysis is not reliable in quantifying microplastics in environmental samples (Fig. 2g). For some other particles, the use of a 785 nm laser may help to weaken the fluorescence (Fig. S7a, h, j). However, the charge-coupled-device (CCD) detector responds poorly to the Raman shift beyond 2000 cm^{-1} excited by 785 nm[39], making it challenging to identify polymers without C-H stretching vibrations at 2800-3200 cm^{-1} (Fig. S7b, c, j). In addition, unlike the Raman shift between 2800-3200 cm^{-1}, which could be selected as the range of autofocus when using a 488 or 532 nm laser, the complete Raman shift can be selected as the range of autofocus, which makes it easy to focus on the glass slide or substrate instead of the particles (Fig. S7c, i, j). Therefore, a 785 nm laser is not recommended in the Raman-based automated analysis of microplastics. Although nonplastic materials are not the focus of this study, we find that coal in the LDIR-based particle analysis is identified as orthoclase by Raman-based particle analysis (Fig. 4b). In summary, Raman-based particle analysis should not be used for the automated analysis of microplastics in environmental samples based on the consideration of strong fluorescence interference, but it may be possible to use this method to quantify the release of microplastics and nanoplastics in daily products[40,41].

Reference databases are crucial in material identification. After decades of development of FTIR and Raman technologies, reference databases for a variety of polymers and polymer additives have been created. However, when identifying microplastics in environmental samples, it is best to use microplastics with environmental characteristics to create a database to address the influence of weathering on FTIR or Raman spectra[7], such as those included in the Spectral Library of Plastic Particles Aged in the Environment (SLoPP-E)[42], the Raman Database of Weathered Microplastics (RDWP)[28] and the FTIR reference database designed for the automated analysis of microplastics[43]. Recently, Open Specy software has been developed for allowing researchers to share, view, process, and identify their spectra for free[44]. Although LDIR-based particle analysis data should theoretically be compatible with the FTIR-based particle analysis database, we suggest that it still needs to be further confirmed and revised in Clarity (version 1.3.42).

Speed

The LDIR-based particle analysis and the Raman-based particle analysis are based on point analysis, so the average time required for measuring a single particle can be calculated and compared (Table 1). It is meaningless to compare the total times required because the number of particles detected differs (Fig. 2). The average measurement time per particle under the LDIR-based particle analysis is approximately 6-9 s, while the average measurement time per particle under the Raman-based particle analysis is 14-15 s. The time used by the Raman-based particle analysis is related to the integration time, cumulation time, Autofocus range and steps.

Only the time required for measuring a certain area (1 mm^2) can be calculated for FPA-FTIR imaging. It takes approximately 2 min to measure 1 mm^2 with the 2×2 binning setting (resolution of 10 μm) and approximately 9 min to measure 1 mm^2 without binning (resolution of 5 μm), approximately 4 times that with 2×2 binning. It takes approximately 7 hours to measure an entire aluminum oxide filter (14.9×15.5 mm, 4×4 binning, Fig. S10). If there are many particles in a small area, FPA-FTIR imaging will be preferred. If there are a few particles in a large area, then particle analysis will be preferred.

Table 1. Time consumption and analysis speed of different strategies.

ID[a]	Strategy	Total (min)	Particle (s)	1 mm^2 (min)
SS #1	LDIR	7.66	6.39	NA[b]
	Raman	82	14.0	NA
	FPA-FTIR (2×2 binning)	179	NA	1.88
ES #1	LDIR	10.5	9.69	NA
	Raman	73	15.5	NA
	FPA-FTIR (2×2 binning)	108	NA	1.92
SS #2	Raman	63	14.3	NA
	FPA-FTIR (2×2 binning)	28	NA	2.38
SS #3	Raman	11.5	11.3	NA
	FPA-FTIR (no binning)	24	NA	9.38

ES #2	Raman	63	14.2	NA
	FPA-FTIR (2×2 binning)	30	NA	2.46

a: Sample ID is written as the abbreviation of the initial character.

b: Not applicable

Submicron sized microplastics (0.5-5 μm)

The Raman mapping (Fig. 5c) and O-PTIR image (Fig. 5d) of PVC particles are the same as the material map created by Raman-based particle analysis (Fig. 5b). Specifically, Raman mapping provides a more detailed description of the edges of particles (Fig. 5c), while Raman-based particle analysis provides a smoother edge measurement (Fig. 5b). Therefore, the particle size measured with Raman-based particle analysis is larger than that measured by Raman mapping. For example, two adjacent microplastic particles (Fig. S11c) were not successfully divided by Raman-based particle analysis (Fig. S11b), but they were successfully divided by Raman mapping (Fig. S11a). The smallest microplastics detected by Raman-based particle analysis is 0.61 μm (Fig. S11b). Raman mapping and O-PTIR imaging can measure the microplastic with a size of about 0.5 μm (Fig. 5j, l). A high-precision motor stage can be used to compensate for the resolution of the Raman spectrum to detect nanoplastics with a size of 30 nm[26,45,46]. Raman mapping and O-PTIR imaging should be suitable for toxicological studies of microplastics and nanoplastics[47]. However, Raman mapping and O-PTIR imaging are challenging to apply to the quantification of microplastics and nanoplastics because it is too slow (Fig. 5b, c, d)[48]. Raman mapping cannot be applied in the analysis of environmental microplastics because of fluorescence interference. O-PTIR can be used to analyze environmental microplastics because it has no risk of fluorescence interference and has the automated potential of adopting the same strategy as LDIR-based particle analysis. Besides, it is a challenge to separate and purify submicron-sized microplastics from environmental matrices[1].

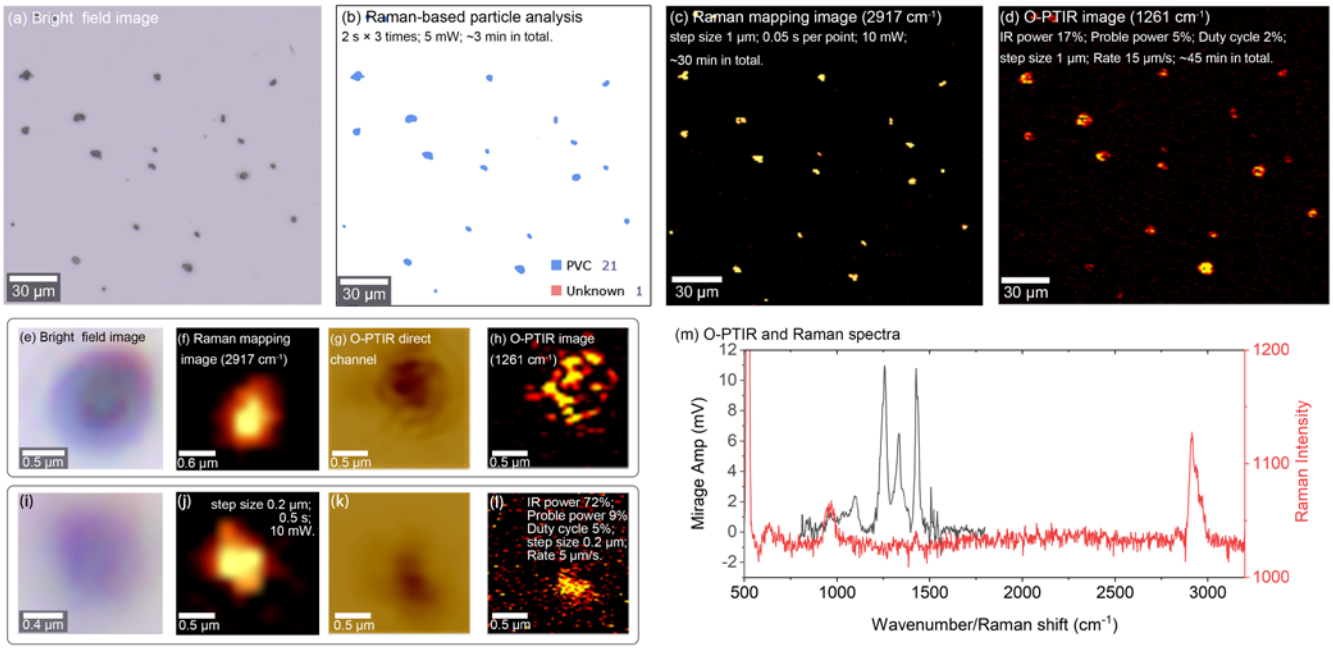

Figure 5. Optical bright field image (a, e, i), Raman mapping image (a, f, j), O-PTIR image (d, g, h, k, l), and material map created by Raman-based particle analysis (b) of PVC particles (standard sample #4). O-PTIR and Raman spectra (m) were measured by the mIRage at the same time. (f) and (h) was measured with the same parameters listed in (j) and (l).

Requirement for sample preparation

The most commonly used method for separating microplastics is filtration[49]. In this case, the choice of the filter membrane is very important[50]. According to the structure, filter membranes can be divided into multilayer/fiber-type (e.g., glass fiber, cellulose nitrate, and cellulose fiber) and monolayer-type (e.g., polycarbonate (PC), and aluminum oxide) membranes[16,49-51]. According to the material, filter membranes can be divided into polymer-type (e.g., nylon, and polyethersulfone) and inorganic membrane-type (e.g., glass fiber) membranes. In LDIR-based particle analysis, the filter membrane first needs to be sonicated in ethanol solution to extract the particles. Ethanol was further concentrated by nitrogen blowing and transferred to Kevley low-E slides. There are two sample transfer steps. It is necessary to use an inorganic single-layer filter membrane (e.g., inorganic aluminum oxide membrane) to avoid contamination or the potential loss of particles trapped inside the filter membrane. If we do not consider the potential contamination that the filter membrane may bring, the nylon filter membrane should also be acceptable because of its low surface adsorption rate[49].

FPA-FTIR imaging accepts the filter membrane to load particles directly but requires that the filter membrane has as little infrared absorption as possible and can be distinguished from microplastic particles by IR imaging. Glass fiber membranes and polymer-type membranes are not applicable. The aluminum oxide filter has been widely used[2,17,51-53] because it has no infrared absorption above 1250 cm^{-1} [51]. The recommend FPA-FTIR imaging uses FPA to measure the transmission spectra of particles loaded on the aluminum oxide (Fig. S10). The machine learning model in Purency Microplastics Finder is trained with the transmission spectrum imaging data obtained with an aluminum oxide membrane[33]. The potential problem is that the largest pore size of the commercial aluminum oxide filter is only 0.2 μm, which is easily blocked during the filtration process[2]. In addition, the particles easily gather at the edge of the filter (Fig. S10), making them indistinguishable. A silicon filter is also suitable for FPA-FTIR imaging[51].

Raman-based particle analysis allows the same sample preparation approach as LDIR-based particle analysis and allows the filter membrane to load particles directly. The filter membrane must be uniform and flat to meet the requirements of dark-field microscopy, confocal microscopy, and polymer analysis, which means that the filter membrane cannot be a polymer-type or fiber-type membrane. Therefore, Raman-based particle analysis cannot use most commercial membranes, including alumina membranes, which is not suitable for dark-field microscopy (Fig. S12). Instead, PC coated with aluminum[16] and a silicon filter[51] are suitable for use in polymer analysis and dark-field microscopy.

ASSOCIATED CONTENT

Supporting Information

The Supporting Information is available free of charge on the website.

The Supporting Information includes the following: Detail information of standard microplastics. Photographs of environmental microplastics, a Kevley low-E slide, and a polished silicon wafer. FTIR spectra of a silicon wafer, Kevley low-E slide, and aluminum oxide filter. Material map of standard samples #1 and #2. Raman spectra of particles measured by 488, 532 and 785 nm lasers.

AUTHOR INFORMATION

Corresponding Authors

* Mingtan Dong - School of Environmental Studies, China University of Geosciences, Wuhan 430078, China; orcid.org/0000-0003-0303-8517; Email: hegu@cug.edu.cn

**Zejiao Luo - School of Environmental Studies, China University of Geosciences, Wuhan 430078, China; orcid.org/0000-0002-0894-815X; Email: zjluo@cug.edu.cn

Author Contributions

Mingtan Dong: Conceptualization, Methodology, Formal analysis, Writing - original draft

Zhenbing She: Resources, Writing - review & editing

Xiong Xiong: Writing - review & editing

Zejiao Luo: Resources, Funding acquisition, Writing - review & editing

Notes

The authors declare no competing financial interest.

ACKNOWLEDGMENT

We acknowledge Agilent Technologies (China) Co., Ltd., Bruker (Beijing) Scientific Technology Co. Ltd., Quantum Design China, Purency GmbH, Photothermal Spectroscopy Corp., and WITec (Beijing) Scientific Technology Co., Ltd, for providing technical support. We acknowledge Guiping Chen, Hailong Hu, Jingjing Wang, Lukas Wander, Michael Stibi, Michael Tang, Mike Lo, Wanghua Wu, William Zhao, Xi Hu and Yang Gao for their assistance in this study. This research was funded by the National Key Research and Development Program (2020YFC1806804).

REFERENCES

(1) Lim, X. *Nature* **2021**, *593*, 22-25.
(2) Bergmann, M.; Mützel, S.; Primpke, S.; Tekman, M. B.; Trachsel, J.; Gerdts, G. *Science Advances* **2019**, *5*, 10.
(3) Ragusa, A.; Svelato, A.; Santacroce, C.; Catalano, P.; Notarstefano, V.; Carnevali, O.; Papa, F.; Rongioletti, M. C. A.; Baiocco, F.; Draghi, S.; D'Amore, E.; Rinaldo, D.; Matta, M.; Giorgini, E. *Environ Int* **2021**, *146*, 106274.
(4) Fred-Ahmadu, O. H.; Bhagwat, G.; Oluyoye, I.; Benson, N. U.; Ayejuyo, O. O.; Palanisami, T. *Sci Total Environ* **2020**, *706*, 135978.
(5) Almeida, M.; Martins, M. A.; Soares, A. M. V.; Cuesta, A.; Oliveira, M. *Environ Toxicol Pharmacol* **2019**, *69*, 57-65.
(6) Prata, J. C.; da Costa, J. P.; Duarte, A. C.; Rocha-Santos, T. *TrAC Trends in Analytical Chemistry* **2019**, *110*, 150-159.
(7) Lenz, R.; Enders, K.; Stedmon, C. A.; Mackenzie, D. M. A.; Nielsen, T. G. *Mar Pollut Bull* **2015**, *100*, 82-91.
(8) Hitchcock, J. N.; Mitrovic, S. M. *Environ Pollut* **2019**, *247*, 457-466.
(9) Xiong, X.; Liu, Q.; Chen, X.; Wang, R.; Duan, M.; Wu, C. *Chemosphere* **2021**, *282*.
(10) Lenaker, P. L.; Baldwin, A. K.; Corsi, S. R.; Mason, S. A.; Reneau, P. C.; Scott, J. W. *Environ Sci Technol* **2019**, *53*, 12227-12237.
(11) Löder, M. G. J.; Gerdts, G. In *Marine Anthropogenic Litter*, 2015, pp 201-227.
(12) Chae, Y.; Kim, D.; An, Y. J. *Aquat Toxicol* **2019**, *216*, 105296.
(13) Feng, J. X.; Zhao, H. S.; Gong, X. Y.; Xia, M. C.; Cai, L. S.; Yao, H.; Zhao, X.; Yan, Z. H.; Li, Z. P.; Nie, H. G.; Ma, X. X.; Zhang, S. C. *Analytical Chemistry* **2021**, *93*, 5521-5528.
(14) Laborda, F.; Trujillo, C.; Lobinski, R. *Talanta* **2021**, *221*, 121486.
(15) Li, Q.; Zeng, A.; Jiang, X.; Gu, X. *J Hazard Mater* **2021**, *412*, 125164.
(16) Ossmann, B. E.; Sarau, G.; Schmitt, S. W.; Holtmannspotter, H.; Christiansen, S. H.; Dicke, W. *Anal Bioanal Chem* **2017**, *409*, 4099-4109.
(17) da Silva, V. H.; Murphy, F.; Amigo, J. M.; Stedmon, C.; Strand, J. *Analytical Chemistry* **2020**, *92*, 13724-13733.
(18) Tagg, A. S.; Sapp, M.; Harrison, J. P.; Ojeda, J. J. *Analytical Chemistry* **2015**, *87*, 6032-6040.
(19) Weisser, J.; Beer, I.; Hufnagl, B.; Hofmann, T.; Lohninger, H.; Ivleva, N. P.; Glas, K. *Water* **2021**, *13*.
(20) Rios Mendoza, L. M.; Balcer, M. *TrAC Trends in Analytical Chemistry* **2019**, *113*, 402-408.
(21) Cowger, W.; Booth, A. M.; Hamilton, B. M.; Thaysen, C.; Primpke, S.; Munno, K.; Lusher, A. L.; Dehaut, A.; Vaz, V. P.; Liboiron, M.; Devriese, L. I.; Hermabessiere, L.; Rochman, C.; Athey, S. N.; Lynch, J. M.; De Frond, H.; Gray, A.; Jones, O. A. H.; Brander, S.; Steele, C., et al. *Appl Spectrosc* **2020**, 3702820930292.
(22) Hartmann, N. B.; Huffer, T.; Thompson, R. C.; Hassellov, M.; Verschoor, A.; Daugaard, A. E.; Rist, S.; Karlsson, T.; Brennholt, N.; Cole, M.; Herrling, M. P.; Hess, M. C.; Ivleva, N. P.; Lusher, A. L.; Wagner, M. *Environ Sci Technol* **2019**, *53*, 1039-1047.
(23) Hale, R. C.; Seeley, M. E.; La Guardia, M. J.; Mai, L.; Zeng, E. Y. *Journal of Geophysical Research: Oceans* **2020**, *125*.
(24) Olson, N. E.; Xiao, Y.; Lei, Z.; Ault, A. P. *Anal Chem* **2020**, *92*, 9932-9939.
(25) Sobhani, Z.; Al Amin, M.; Naidu, R.; Megharaj, M.; Fang, C. *Anal Chim Acta* **2019**, *1077*, 191-199.
(26) Sobhani, Z.; Zhang, X.; Gibson, C.; Naidu, R.; Megharaj, M.; Fang, C. *Water Research* **2020**, *174*.
(27) Stock, V.; Böhmert, L.; Lisicki, E.; Block, R.; Cara-Carmona, J.; Pack, L. K.; Selb, R.; Lichtenstein, D.; Voss, L.; Henderson, C. J.; Zabinsky, E.; Sieg, H.; Braeuning, A.; Lampen, A. *Archives of Toxicology* **2019**, *93*, 1817-1833.
(28) Dong, M.; Zhang, Q.; Xing, X.; Chen, W.; She, Z.; Luo, Z. *Sci Total Environ* **2020**, *739*, 139990.
(29) Anger, P. M.; von der Esch, E.; Baumann, T.; Elsner, M.; Niessner, R.; Ivleva, N. P. *TrAC Trends in Analytical Chemistry* **2018**, *109*, 214-226.
(30) Löder, M. G. J.; Kuczera, M.; Mintenig, S.; Lorenz, C.; Gerdts, G. *Environmental Chemistry* **2015**, *12*.
(31) Simon, M.; van Alst, N.; Vollertsen, J. *Water Res* **2018**, *142*, 1-9.
(32) Wander, L.; Vianello, A.; Vollertsen, J.; Westad, F.; Braun, U.; Paul, A. *Analytical Methods* **2020**, *12*, 781-791.
(33) Hufnagl, B.; Steiner, D.; Renner, E.; Löder, M. G. J.; Laforsch, C.; Lohninger, H. *Analytical Methods* **2019**, *11*, 2277-2285.
(34) Primpke, S.; Cross, R. K.; Mintenig, S. M.; Simon, M.; Vianello, A.; Gerdts, G.; Vollertsen, J. *Appl Spectrosc* **2020**, *74*,

1127-1138.
(35) Reffner, J. A. **2018**.
(36) Beltran, V.; Marchetti, A.; Nuyts, G.; Leeuwestein, M.; Sandt, C.; Borondics, F.; De Wael, K. *Angew Chem Int Ed Engl* **2021**.
(37) Li, L.; Zhao, X.; Li, Z.; Song, K. *J Hazard Mater* **2021**, *411*, 124955.
(38) Scircle, A.; Cizdziel, J. V.; Tisinger, L.; Anumol, T.; Robey, D. *Toxics* **2020**, *8*.
(39) Toporski, J.; Dieing, T.; Hollricher, O. *Confocal Raman Microscopy*; Springer, 2018; Vol. 66.
(40) Xu, J.-L.; Lin, X.; Hugelier, S.; Herrero-Langreo, A.; Gowen, A. A. *Journal of Hazardous Materials* **2021**, *418*.
(41) Li, D.; Shi, Y.; Yang, L.; Xiao, L.; Kehoe, D. K.; Gun'ko, Y. K.; Boland, J. J.; Wang, J. J. *Nature Food* **2020**, *1*, 746-754.
(42) Munno, K.; De Frond, H.; O'Donnell, B.; Rochman, C. M. *Analytical Chemistry* **2020**, *92*, 2443-2451.
(43) Primpke, S.; Wirth, M.; Lorenz, C.; Gerdts, G. *Anal Bioanal Chem* **2018**, *410*, 5131-5141.
(44) Cowger, W.; Steinmetz, Z.; Gray, A.; Munno, K.; Lynch, J.; Hapich, H.; Primpke, S.; De Frond, H.; Rochman, C.; Herodotou, O. *Anal Chem* **2021**, *93*, 7543-7548.
(45) Fang, C.; Sobhani, Z.; Zhang, X.; Gibson, C. T.; Tang, Y.; Naidu, R. *Water Res* **2020**, *183*, 116046.
(46) Fang, C.; Sobhani, Z.; Zhang, X.; McCourt, L.; Routley, B.; Gibson, C. T.; Naidu, R. *Water Res* **2021**, *194*, 116913.
(47) Ramsperger, A.; Narayana, V. K. B.; Gross, W.; Mohanraj, J.; Thelakkat, M.; Greiner, A.; Schmalz, H.; Kress, H.; Laforsch, C. *Sci Adv* **2020**, *6*.
(48) Kappler, A.; Fischer, D.; Oberbeckmann, S.; Schernewski, G.; Labrenz, M.; Eichhorn, K. J.; Voit, B. *Anal Bioanal Chem* **2016**, *408*, 8377-8391.
(49) Cai, H.; Chen, M.; Chen, Q.; Du, F.; Liu, J.; Shi, H. *Chemosphere* **2020**, *257*.
(50) Süssmann, J.; Krause, T.; Martin, D.; Walz, E.; Greiner, R.; Rohn, S.; Fischer, E. K.; Fritsche, J. *Food Control* **2021**, *125*.
(51) Kappler, A.; Windrich, F.; Loder, M. G.; Malanin, M.; Fischer, D.; Labrenz, M.; Eichhorn, K. J.; Voit, B. *Anal Bioanal Chem* **2015**, *407*, 6791-6801.
(52) Mintenig, S. M.; Int-Veen, I.; Loder, M. G. J.; Primpke, S.; Gerdts, G. *Water Res* **2017**, *108*, 365-372.
(53) Primpke, S.; Lorenz, C.; Rascher-Friesenhausen, R.; Gerdts, G. *Analytical Methods* **2017**, *9*, 1499-1511.

Table of Contents artwork